

Epitaxial stabilization of SrCu_3O_4 with infinite $\text{Cu}_{3/2}\text{O}_2$ layers

Hiroshi Takatsu,[†] Masayuki Ochi,[‡] Naoya Yamashina,[†] Morito Namba,[†] Kazuhiko Kuroki,[‡] Takahito Terashima,[¶] and Hiroshi Kageyama^{*,†}

[†]*Department of Energy and Hydrocarbon Chemistry, Graduate School of Engineering, Kyoto University, Kyoto 615-8510, Japan*

[‡]*Department of Physics, Osaka University, Machikaneyama-cho, Toyonaka, Osaka 560-0043, Japan*

[¶]*Department of Physics, Graduate School of Science, Kyoto University, Kyoto 606-8502, Japan*

E-mail: kage@scl.kyoto-u.ac.jp

Abstract

We report the epitaxial thin film synthesis of SrCu_3O_4 with infinitely stacked Cu_3O_4 layers composed of edge-sharing CuO_4 square-planes, using molecular beam epitaxy. Experimental and theoretical characterizations showed that this material is a metastable phase that can exist by applying tensile biaxial strain from the (001)- SrTiO_3 substrate. SrCu_3O_4 shows an insulating electrical resistivity in accordance with the Cu^{2+} valence state revealed X-ray photoelectron spectroscopy. First-principles calculations also indicated that the unoccupied $d_{3z^2-r^2}$ band becomes substantially stabilized owing to the absence of apical anions, in contrast to $\text{A}_2\text{Cu}_3\text{O}_4\text{Cl}_2$ ($A = \text{Sr}, \text{Ba}$) with an A_2Cl_2 block layer and therefore a *trans*- CuO_4Cl_2 octahedron. These results suggest that SrCu_3O_4 is a suitable parent material for electron-doped superconductivity based on the Cu_3O_4 plane.

Introduction

The discovery of superconductivity in $\text{La}_{2-x}\text{Ba}_x\text{CuO}_4$ ¹ has led to intensive research to explore layered cupric compounds with high T_c 's.²⁻⁶ They universally possess two-dimensional (2D) CuO_2 planes with an apex-linked CuO_4 square-planar coordination, sandwiched by blocking layers (e.g., LaO layers in La_2CuO_4 ⁶ and BaO layers in $\text{YBa}_2\text{Cu}_3\text{O}_6$ ⁷). Superconductivity is observed when appropriate carriers are injected to the 'parent' Cu^{2+}O_2 plane. Carrier doping can usually be done via aliovalent substitution or by creating defects in the blocking layers.

Despite extensive research, most cuprate superconductors are hole-doped, and only a handful electron-doped materials have been reported. In the electron-doped case, the absence of apical anions in the CuO_2 plane is considered as essential.^{2,5} $A\text{CuO}_2$ (A = alkaline earth metals),^{8,9} which consists of infinitely stacked CuO_2 planes, $[\text{CuO}_2]_\infty$, separated only by A cations, is therefore the ideal host system. High-pressure synthesis and thin film growth techniques allow the expansion of accessible compositional range. For example, thin film studies show superconductivity upon electron doping, namely in the infinite layer (IL) $\text{Sr}_{1-x}\text{Ln}_x\text{CuO}_2$ ($\text{Ln} = \text{La}, \text{Nd}$) with $T_c \sim 40$ K.^{10,11} More recently, the isoelectric nickel oxide film has been shown to exhibit superconductivity at about 10 K.¹²

In parallel with compounds having CuO_2 planes, different structural motifs have been explored.^{13,14} In particular, the $\text{Cu}_{3/2}\text{O}_2$ (or Cu_3O_4) plane in $A_2\text{Cu}_3\text{O}_4\text{Cl}_2$ ($A = \text{Sr}, \text{Ba}$), characterized by a periodic insertion of 1/2 Cu in the CuO_2 plane (Figure 1b, right), has attracted attention,¹³ since the Cu arrangement in the Cu_3O_4 plane is reminiscent of a line-centered square lattice known as the Lieb lattice,¹⁵ and electron-doped superconductivity is suggested. Unfortunately, the blocking $A_2\text{Cl}_2$ layer in $A_2\text{Cu}_3\text{O}_4\text{Cl}_2$ provides apical (Cl) anions to $\text{Cu}(1)$, resulting in *trans*- CuO_4Cl_2 octahedra (Figure 1a), which is thus unsuitable for electron-doped superconductivity. In fact, the absence of superconductivity in hole-doped $\text{Ba}_2\text{Cu}_3\text{O}_4\text{Cl}_2$ has been discussed in terms of hole localization at the apical ligand.^{16,17} It is thus crucial to explore materials with the Cu_3O_4 plane without apical anions.

This paper reports on the thin film growth of SrCu_3O_4 , using molecular beam epitaxy (MBE). In contrast to $\text{A}_2\text{Cu}_3\text{O}_4\text{Cl}_2$, this compound epitaxially grown on a SrTiO_3 substrate is composed of infinite layers of $\text{Cu}_{3/2}\text{O}_2$ (Cu_3O_4) separated only by Sr cations. First-principles calculations verify that the biaxial tensile strain from the substrate stabilize SrCu_3O_4 against competing phases of “ $\text{SrCu}_2\text{O}_3 + \text{CuO}$ ”. Furthermore, the $d_{3z^2-r^2}$ orbitals become substantially stabilized, making SrCu_3O_4 a unique candidate for electron-doped superconductor based on the Cu_3O_4 lattice.

Experiments and Calculations

Target films were grown on (001)- SrTiO_3 single crystalline substrates using a custom-made reactive MBE system (EGL-1420-E2, Biemtron). Elemental Sr and Cu fluxes were simultaneously provided from conventional Knudsen cells typically with flux rates of 0.05 \AA/s for Sr and 0.02 \AA/s for Cu, as determined by an INFICON quartz crystal microbalance system before the growth. These rates approximately correspond to the nominal composition of Sr:Cu = 1:2. Ozone gas was supplied using a commercial ozonizer with a background pressure of 4×10^{-6} Torr. After annealing the substrates at about $700 \text{ }^\circ\text{C}$ for 2–4 hours in vacuum, the temperature, monitored by an optical pyrometer with the wavelength of $\lambda = 8\text{--}13 \text{ }\mu\text{m}$ (IR-CAI3TS, CHINO), was set at $472 \text{ }^\circ\text{C}$. The surface structure of the film and the substrate was monitored *in-situ* by reflection high-energy electron diffraction (RHEED) with an acceleration voltage of 20 keV.

X-ray diffraction (XRD) measurements after the growth were carried out at room temperature (RT) using a Rigaku SmartLab diffractometer equipped with a $\text{Cu K}\alpha_1$ monochromator. The scanning transmission electron microscopy (STEM) observation and chemical composition analysis were conducted using a JEOL transmission electron microscope (JEM-ARM200F) at an operating voltage of 200 kV equipped with an energy dispersive X-ray spectrometer (JED-2300T SDD). Incident electron beam along the stacking direction of the

film was transmitted through a hole made by removing the substrate by Ar-ion beam milling. The valence state of copper was investigated by means of X-ray photoelectron spectroscopy (XPS) with Mg K α radiation ($h\nu = 1253.6$ eV; Ulvac-Phi Model5500). The binding energies (E_B) of each XPS spectrum with potential extrinsic E_B shifts caused by the charging effect were calibrated with the adventitious C 1s peak at 284.5 eV. As a reference of divalent copper, XPS spectra for powder samples of SrCuO₂ and SrCu₂O₃ prepared under the reported conditions^{9,14} were collected. The electrical resistivity ρ was measured by using a standard four-probe method. Magnetization measurements were performed with a commercial superconducting quantum interference device (SQUID) magnetometer (magnetic property measurement system (MPMS), Quantum Design).

To examine structural stability and electronic properties, we performed first-principles calculations using the projector augmented wave method¹⁸ as implemented in the Vienna *ab initio* simulation package (VASP).¹⁹⁻²² We used the Perdew-Burke-Ernzerhof parametrization of the generalized gradient approximation (PBE-GGA)²³ without the spin-orbit coupling. For calculations of the total energy and the phonon dispersion, we optimized the crystal structure until the Hellmann-Feynman force acting on each atom becomes less than 0.01 eV \AA^{-1} . The plane-wave cutoff energy was 550 eV, and $10 \times 4 \times 10$, $10 \times 14 \times 10$, and $10 \times 10 \times 10$ k -meshes were used for CuO, SrCu₂O₃, and SrCu₃O₄, respectively. To calculate the phonon dispersion, we assumed for simplicity a non-magnetic state using a $3 \times 3 \times 3$ q -mesh, using the experimental lattice constants of the thin film ($a = 5.42$ \AA and $c = 3.53$ \AA). The finite displacement method, as implemented in the Phonopy software,²⁴ was used. The (non-magnetic) electronic band dispersion of SrCu₃O₄ was obtained using the structural parameters obtained by our experiments.

Result and discussion

We initially investigated the crystal structure of the obtained film on the SrTiO₃ substrate using high-resolution XRD. The out-of-plane θ - 2θ pattern shows peaks around $2\theta = 25^\circ$ and 52° , suggesting the growth of well-oriented epitaxial films (Supporting Information, Figure S1). The out-of-plane lattice constant was estimated to be 3.53 Å, slightly larger than the bulk samples of IL-SrCuO₂ (3.432 Å)⁹ and spin-ladder SrCu₂O₃ (3.495 Å),¹⁴ both composed of Cu²⁺-O layers with Sr²⁺ cations in between. Distinct fringes in the XRD profile (Figure S1) indicate the atomic scale smoothness of the interface between the substrate and the film. The spacing of fringes gave a film thickness of about 30 nm, in agreement with that estimated from the growth rate. The rocking curve of the peak around 25° gave a full width at half-maximum (FWHM) value of $\Delta\omega = 0.09^\circ$, indicating excellent film quality. No target phase was observed when KTaO₃ and DyScO₃ substrates with larger strain (vs. SrTiO₃) were used under the same growth conditions (Supporting Information, Figure S2).

To clarify the in-plane structure of the film, we conducted STEM experiments. Figure 2a shows a high-angle annular dark-field (HAADF) STEM image for a 30 nm thickness sample, highlighting the atomic position of Sr and Cu corresponding, respectively, to bright and dark spots. The line scans in Figure 2b demonstrate the change in intensity I at Sr and Cu positions. Since I is proportional to the average atomic number Z of the projected atomic column and scales as $I \sim Z^n$ ($n = 1.6$ – 1.9), these scans can distinguish between Sr and Cu atoms. The observed pattern is different from those expected from the CuO₂ plane (Figure 1b, left) and the BaCu₃O₄-type structure,²⁵ but instead suggests the formation of Cu₃O₄ (Cu_{3/2}O₂) planes (Figure 1b, right), as found in A₂Cu₃O₄Cl₂, leading to SrCu₃O₄. Annular bright-field scanning transmission electron microscopy (ABF-STEM) is also consistent with the formation of Cu₃O₄ (Cu_{3/2}O₂) planes (Figure 2c). Note that EDX analysis exhibited a slightly smaller atomic ratio of Cu/Sr $\simeq 2.5$, probably due to the influence of surface impurity phases, as will be shown later. The corresponding electron diffraction along the c axis (i.e., perpendicular to the substrate) shows a four-fold symmetry with an in-plane lattice

constant of $a = 5.42 \text{ \AA}$ (Supporting Information, Figure S3), which is consistent with the STEM image. The right panel of Figure 1a shows the most plausible structure of SrCu_3O_4 with the $P4/mmm$ space group (No. 123), where Sr is at the 1b site, Cu at the 1c and 2f sites, and O at the 4j site (Supporting Information, Table S1). The in-plane cell is related to the substrate (SrTiO_3 perovskite) by $\sqrt{2}a \times \sqrt{2}a$, as depicted in Figure 2c.

The X-ray reciprocal space mapping (RSM) in Figure 3a shows a peak around $2\theta = 30.2^\circ$ and $\chi = 33.1^\circ$, corresponding to the 101 reflection of SrCu_3O_4 . Known Sr-Cu-O compounds including Sr_2CuO_3 ,²⁶ SrCuO_2 ,⁹ $\text{Sr}_{14}\text{Cu}_{24}\text{O}_{41}$,²⁷ SrCu_2O_2 ,²⁸ and $\text{Sr}_{n-1}\text{Cu}_{n+1}\text{O}_{2n}$ ($n = 3, 5$)¹⁴ exhibit no reflection at this 2θ angle. The azimuthal ϕ scan for the 101 reflection showing four peaks separated by 45° from the 101 peaks of the SrTiO_3 substrate (Figures 3c and 3e) is consistent with the STEM image (Figures 2a and 2c). Coherent growth of the film on the substrate is confirmed by the RSM around the 113 reflection (Figure 3b), and such coherent growth is reproduced in other films (Supporting Information, Figure S4). The in-plane lattice constant estimated from RSM measurements, $a = \sqrt{2} \times 3.90 = 5.52 \text{ \AA}$, was found to be 2% more tensile-strained than that estimated from ED measurements ($a = 5.42 \text{ \AA}$, Supporting Information, Table S2), as a consequence of the removal of the SrTiO_3 substrate to observe the in-plane structure for ED measurements. Other reflections, such as 111, 131, and 202, are also compatible with the crystal symmetry of the SrCu_3O_4 structure (Figure 3d). SrCu_3O_4 is the first experimental realization of Cu_3O_4 infinite layers (Figure 1a and 1b, right). We note that the orthorhombic BaCu_3O_4 also has a layer of the Cu_3O_4 composition, but is composed of diamond chains (or diagonal ladders).^{25,29}

Using the lattice constants of $a = 5.42 \text{ \AA}$ and $c = 3.53 \text{ \AA}$ determined by XRD and STEM observations, we performed bond valence sum calculations and obtained +2.13 for Sr and +1.94 for Cu, in accordance with the formal valences of Sr^{2+} and Cu^{2+} . Figure 4a shows the $2p$ -core-level XPS spectrum of Cu in a SrCu_3O_4 film (5 nm thickness), plotted with SrCuO_2 , SrCu_2O_3 , Cu_2O , and CuO .⁶ The spectrum has distinct satellite peaks separated by $\sim 9 \text{ eV}$, thus being reasonably ascribed to the divalent copper state.

Figure 4b shows the temperature dependence of the in-plane electrical resistivity ρ of the SrCu₃O₄ film with 30 nm thickness. It shows an insulating behavior in the temperature range from 400 to 270 K, but ρ was too large to measure at lower temperatures. Impurity scattering from defects and impurities will have a negligible effect on the resistivity in the temperature range currently measured.³¹ The ρ - T curve can thus be fitted well by a variable range hopping in 2D ($d = 2$), $\rho(T) = \rho_0 \exp(T_0/T)^{1/d+1}$, implying carrier hopping in the Cu₃O₄ plane. A₂Cu₃O₄Cl₂ with the Cu₃O₄ plane exhibits a canted antiferromagnetic phase transition of Cu(1) spins at $T_N = 380$ K ($A = \text{Sr}$)³² and 332 K ($A = \text{Ba}$).³³ No sign of antiferromagnetic phase transition is seen in the resistivity and magnetization data collected at $270 \text{ K} < T < 400 \text{ K}$ and $5 \text{ K} < T < 400 \text{ K}$, respectively, although SrCu₃O₄ is expected to be a Mott insulator. This is because it is difficult to probe antiferromagnetic order using thin films.

Let us discuss why the present MBE method has enabled the stabilization of SrCu₃O₄. In general, MBE growth provides near thermal equilibrium conditions, with much smaller kinetic energy than other growth techniques such as pulsed laser deposition and sputtering.^{34,35} For this reason, the synthesis of SrCu₃O₄ cannot be explained in terms of kinetic trapping. On the other hand, epitaxial strain from the substrate is the most likely source for the SrCu₃O₄ phase formation.^{8,10} This scenario is consistent with the observation that SrCu₃O₄ is formed only when the film thickness is less than 30 nm. For thicker films, impurity phases such as SrCu₂O₃ and CuO were observed in the STEM and RHEED images (Figure S5) and in the XPS data for the 30 nm film (Figure S6). In addition, finely tuned conditions are required (Supporting Information, Table S3); SrCu₃O₄ can be prepared with a narrow growth window of temperature ($T = 472 \pm 1$ °C) and Cu/Sr ratio (nominal ratio of Cu/Sr = 2 ± 0.3).

First-principles calculations were conducted to theoretically address the stability of SrCu₃O₄, in comparison with competing phases of SrCu₂O₃ and CuO. In an early stage of calculations, it was found that SrCu₃O₄ does not have an imaginary mode in the phonon dispersion when

calculated using experimental lattice constants (Figure S7). However, the total energy of SrCu_3O_4 is higher than that of “ $\text{SrCu}_2\text{O}_3 + \text{CuO}$ ” by 0.19 eV per formula unit (here all the structural parameters were optimized), meaning that SrCu_3O_4 is dynamically stable (or structurally stable as one of the possible structures in the Sr-Cu-O composition) but not the most thermodynamically stable. In other words, this material cannot form in bulk owing to competing phases found in the Sr-Cu-O phase diagram.^{3-5,41} It is interesting to compare the stability between SrCu_3O_4 and the competing SrCu_2O_3 from the structural perspective. SrCu_3O_4 consists only of edge-sharing CuO_4 square planes, whereas SrCu_2O_3 has both edge- and corner-sharing CuO_4 square planes.¹⁴ Thus, the former structure appears to be more energetically unfavorable according to Pauling’s third rule.⁴² However, when tensile strain is applied to SrCu_3O_4 , the Cu_3O_4 layer is stretched and the Cu-Cu repulsion between the edge-sharing CuO_4 square planes is relaxed.

We further compared the total energies of “ SrCu_3O_4 ” and “ $\text{SrCu}_2\text{O}_3 + \text{CuO}$ ” in the presence of epitaxial biaxial strain. To do this, in-plane lattice constants were fixed to the ‘normalized’ substrate lattice constant a_0 (where $a = b = \sqrt{2}a_0$ for SrCu_3O_4 and $a = c = a_0$ for SrCu_2O_3), and other structural parameters were optimized. The strain effect for CuO was not taken into account since CuO was found as an island on the film surface (Figure S5a). When biaxial strain is turned on (i.e., a_0 is varied), the relative energy of SrCu_3O_4 , $E(\text{SrCu}_3\text{O}_4) - E(\text{SrCu}_2\text{O}_3) - E(\text{CuO})$, shows a parabolic shape with negative values for $3.91 \text{ \AA} < a_0 < 3.96 \text{ \AA}$ (Figure 5). The minimum is found at around 3.93 \AA , which is close to the lattice constant of SrTiO_3 (3.905 \AA) used as the substrate, suggesting that adequate tensile strain can stabilize the metastable phase of SrCu_3O_4 . The appearance of SrCu_2O_3 and CuO impurities for thicker films ($> 30 \text{ nm}$) would be due to some relaxation of the SrCu_3O_4 film from the substrate strain, as the film thickness increases. It is naturally considered that multiple domain formation can reduce the stress from the substrate.^{7,8} In this case, when the film thickness exceeds the critical value, the epitaxially stable phase and bulk stable phase grow simultaneously.⁷ This is another strain relaxation mechanism

different from the misfit dislocations that appear in the film-substrate interface.^{9,10} Cross-sectional TEM images will provide detailed features of the domain formations and other possible dislocations along the growth direction, which will be left for future studies.

Finally, we discuss the difference in electronic structures between SrCu_3O_4 and $\text{A}_2\text{Cu}_3\text{O}_4\text{Cl}_2$. Here, the main purpose of the band structure calculation is to see the band width of the $d_{x^2-y^2}$ orbital between Cu(1) and Cu(2), and the energy difference between $d_{x^2-y^2}$ and $d_{3z^2-r^2}$ orbitals. We thus performed the calculation assuming a non-magnetic and metallic state because otherwise the band width and the energy difference are strongly affected by the size of exchange splitting and become spin-dependent. The calculated band dispersion for “non-magnetic” SrCu_3O_4 near the Fermi energy (Figure 6a, 6b) show that the wide band from Cu(1) $d_{x^2-y^2}$ orbitals and the narrow band from Cu(2) $d_{x^2-y^2}$ orbitals are nearly decoupled, as found in $\text{A}_2\text{Cu}_3\text{O}_4\text{Cl}_2$.⁴⁵ Furthermore, the $d_{3z^2-r^2}$ bands of SrCu_3O_4 are substantially stabilized (Figure 6c, 6d) owing to the square-planar coordination, in contrast to $\text{A}_2\text{Cu}_3\text{O}_4\text{Cl}_2$ containing chloride anions at the apical Cu(1) site. This means that SrCu_3O_4 is an ideal 2D system with half-filled $d_{x^2-y^2}$ orbitals on the Cu_3O_4 lattice, where electron-doped superconductivity may occur because the absence of apical anions is known to be crucial for electron-doped superconductivity in the CuO_2 case.^{2,5} If electron doping is possible in SrCu_3O_4 , the absence of apical anions at the Cu(1) site is expected to prevent carrier localization, as observed in the CuO_2 system.^{16,17} The “inserted” Cu(2) may bring about an exotic superconducting state or magnetic ground state, for example, by ferromagnetic fluctuations introduced through 90°-type Cu(1)–O–Cu(2) interaction. Electron doping by chemical substitution, as demonstrated in La- or Nd-substituted IL- SrCuO_2 ^{2,10,11} and electric field gating⁴⁶ in SrCu_3O_4 films, would be an interesting subject in the future.

Conclusion

We have succeeded in synthesizing SrCu₃O₄ thin films on a SrTiO₃ substrate using molecular beam epitaxy. SrCu₃O₄ consists of infinitely stacked Cu_{3/2}O₂ (Cu₃O₄) planes separated only by Sr cations, in contrast to A₂Cu₃O₄Cl₂ (A = Sr, Ba) with the A₂Cl₂ block layer. Experimental and theoretical investigations revealed that this material is a metastable phase that can exist by applying suitable tensile biaxial strain from the substrate. Thus stabilized SrCu₃O₄ shows an insulating behavior, as expected from the formal Cu²⁺ valence. The band structure with substantially stabilized (unoccupied) $d_{3z^2-r^2}$ orbitals (vs A₂Cu₃O₄Cl₂) owing to the absence of apical anions suggests that this material is a suitable parent material for electron-doped superconductivity based on the Cu₃O₄ lattice.

Associated content

Supporting Information Available

Additional information on results of X-ray diffraction, electron diffraction, HAADF-STEM, XPS, and calculations of phonon dispersion of SrCu₃O₄.

Acknowledgement

This work was supported by CREST (JPMJCR1421) and JSPS KAKENHI Grants (No. 17H04849, No. 17H05481, No. JP18H01860, and No. JP18K13470, No.19H04697, No.20H00384).

References

- (1) Bednorz, J. G.; Müller, K. A. Possible high- T_c superconductivity in the Ba–La–Cu–O system. *Z. Phys. B* **1986**, *64*, 189.

- (2) Armitage, N. P.; Fournier, P.; Greene, R. L. Progress and perspectives on electron-doped cuprates. *Rev. Mod. Phys.* **2010**, *82*, 2421.
- (3) Chu, C. W.; Deng, L. Z.; Lv, B. Hole-doped cuprate high temperature superconductors. *Physica C* **2015**, *514*, 290.
- (4) Keimer, B.; Kivelson, S. A.; Norman, M. R.; Uchida, S.; Zaanen, J. From quantum matter to high-temperature superconductivity in copper oxides. *Nature* **2015**, *518*, 179.
- (5) Tokura, Y.; Takagi, H.; Uchida, S. A superconducting copper oxide compound with electrons as the charge carriers. *Nature* **1989**, *337*, 345.
- (6) Tokura, Y.; Arima, T. New Classification Method for Layered Copper Oxide Compounds and Its Application to Design of New High T_c Superconductors. *Jpn. J. Appl. Phys.* **1990**, *29*, 2388.
- (7) Wu, M. K.; Ashburn, J. R.; Torng, C. J. Superconductivity at 93 K in a New Mixed-Phase Y-Ba-Cu-O Compound System at Ambient Pressure. *Phys. Rev. Lett.* **1987**, *58*, 908.
- (8) Siegrist, T.; Zahurak, S. M.; Murphy, D. W.; Roth, R. S. The parent structure of the layered high-temperature superconductors. *Nature* **1988**, *334*, 231.
- (9) Takano, M.; Takeda, Y.; Okada, H.; Miyamoto, M.; Kusaka, T. $ACuO_2$ (A: alkaline earth) crystallizing in a layered structure. *Physica C* **1989**, *159*, 375.
- (10) Smith, M. G.; Manthiram, A.; Zhou, J.; Goodenough, J. B.; Markert, J. T. Electron-doped superconductivity at 40 K in the infinite-layer compound $Sr_{1-y}Nd_yCuO_2$. *Nature* **1991**, *351*, 549.
- (11) Er, G.; Kikkawa, S.; Kanamaru, F.; Miyamoto, Y.; Kanamaru, F.; Tanaka, S.; Sera, M.;

- Sato, M.; Hiroi, Z.; Takano, M.; Bando, Y. Structural, electrical and magnetic studies of infinite-layered $\text{Sr}_{1-x}\text{La}_x\text{CuO}_2$ superconductor. *Physica C* **1992**, *196*, 271.
- (12) Li, D.; Lee, K.; Wang, B. Y.; Osada, M.; Crossley, S.; Lee, H. R.; Cui, Y.; Hikita, Y.; Hwang, H. Y. Superconductivity in an infinite-layer nickelate. *Nature* **2019**, *572*, 624.
- (13) Müller-Buschbaum, H. Oxometallates with Planar Coordination. *Angew. Chem. Int. Ed. Engl.* **1977**, *16*, 674.
- (14) Hiroi, Z.; Azuma, M.; Takano, M.; Bando, Y. A New Homologous Series $\text{Sr}_{n-1}\text{Cu}_{n+1}\text{O}_{2n}$ Found in the SrO-CuO System Treated under High Pressure. *J. Solid State Chem.* **1991**, *95*, 230.
- (15) Lieb, E. H. Two Theorems on the Hubbard Model. *Phys. Rev. Lett.* **1989**, *62*, 1201.
- (16) Noro, S.; Suzuki, H.; Yamaday, T. Magnetic properties of $\text{Ba}_{2-x}\text{K}_x\text{Cu}_3\text{O}_4\text{Cl}_2$. *Solid State Commun.* **1990**, *76*, 711.
- (17) Kato, M.; Tanaami, T.; Koike, Y. Carrier Doping into $(\text{Sr},\text{Ba})_2\text{Cu}_3\text{O}_4(\text{Cl},\text{Br})_2$ with the Cu_3O_4 Plane. *J. Jpn. Soc. Powder and Powder Metallurgy* **2000**, *47*, 1120.
- (18) Kresse, G.; Joubert, D. From ultrasoft pseudopotentials to the projector augmented-wave method. *Phys. Rev. B* **1999**, *59*, 1758.
- (19) Kresse, G.; Hafner, J. Ab initio molecular dynamics for liquid metals. *Phys. Rev. B* **1993**, *47*, 558.
- (20) Kresse, G.; Hafner, J. Ab initio molecular-dynamics simulation of the liquid-metal amorphous-semiconductor transition in germanium. *Phys. Rev. B* **1994**, *49*, 14251.
- (21) Kresse, G.; Furthmüller, J. Efficiency of ab-initio total energy calculations for metals and semiconductors using a plane-wave basis set. *Comput. Mater. Sci.* **1996**, *6*, 15.

- (22) Kresse, G.; Furthmüller, J. Efficient iterative schemes for ab initio total-energy calculations using a plane-wave basis set. *Phys. Rev. B* **1996**, *54*, 11169.
- (23) Perdew, J. P.; Burke, K.; Ernzerhof, M. Generalized Gradient Approximation Made Simple. *Phys. Rev. Lett.* **1996**, *77*, 3865.
- (24) Togo, A.; Tanaka, I. First principles phonon calculations in materials science. *Scr. Mater.* **2015**, *108*, 1.
- (25) Bertinotti, A.; Hammann, J.; Luzet, D.; Vincent, E. Structure of a new type of satellite phase in $\text{YBa}_2\text{Cu}_3\text{O}_{7-\delta}$. *Physica C* **1989**, *160*, 227.
- (26) Liang, J.; Chen, Z.; Wu, F.; Xie, S. Phase diagram of SrO-CaO-CuO ternary system. *Solid State Commun.* **1990**, *75*, 247.
- (27) McCarron, E. M.; Subramanian, M. A.; Calabrese, J. C.; Harlow, R. L. The incommensurate structure of $(\text{Sr}_{14-x}\text{Ca}_x)\text{Cu}_{24}\text{O}_{41}$ ($0 < x < 8$) a superconductor byproduct. *Mat. Res. Bull.* **1988**, *23*, 1355.
- (28) Teske, C. L.; Müller-Buschbaum, H. Zur Kenntnis von SrCu_2O_2 . *Z. Anorg. Allg. Chem.* **1970**, *379*, 113.
- (29) Rischau, C. W.; Leridon, B.; Colson, D.; Forget,; Monod, P. BaCu_3O_4 : High-temperature magnetic order in one-dimensional $S = 1/2$ diamond chains. *Phys. Rev. B* **2012**, *85*, 134518.
- (6) Hayez, V.; Franquet, A.; Hubin, A.; Terryn, H. XPS study of the atmospheric corrosion of copper alloys of archaeological interest. *Surf. Interface Anal.* **2004**, *36*, 876.
- (31) Lee, P. A.; Ramakrishnan, T. V. Disordered electronic systems. *Rev. Mod. Phys.* **1985**, *57*, 287.

- (32) Chou, F. C.; Aharony, A.; Birgeneau, R. J.; Entin-Wohlman, O.; Greven, M.; Harris, A. B.; Kastner, M. A.; Kim, Y. J.; Kleinberg, D. S.; Lee, Y. S.; Zhu, Q. Ferromagnetic Moment and Spin Rotation Transitions in Tetragonal Antiferromagnetic $\text{Sr}_2\text{Cu}_3\text{O}_4\text{Cl}_2$. *Phys. Rev. Lett.* **1997**, *78*, 535.
- (33) Ito, T.; Yamaguchi, H.; Oka, K. Anisotropic magnetization characteristic of Cu_3O_4 planes in $\text{Ba}_2\text{Cu}_3\text{O}_4\text{Cl}_2$. *Phys. Rev. B* **1997**, *55*, R684.
- (34) Schlom, D. G.; Chen, L.-Q.; Pan, X.; Schmehl, A.; Zurbuchen, M. A. A Thin Film Approach to Engineering Functionality into Oxides. *J. Am. Ceram. Soc.* **2008**, *91*, 2429.
- (35) Oka, D.; Fukumura, T. Crystal engineering for novel functionalities with oxide thin film epitaxy. *Cryst. Eng. Comm.* **2017**, *19*, 2144.
- (8) Gorbenko, O. Y.; Samoilenkov, S. V.; Graboy, I. E.; Kaul, A. R. Epitaxial Stabilization of Oxides in Thin Films. *Chem. Mater* **2002**, *14*, 4026.
- (10) Freund, L. B.; Suresh, S. *Thin Film Materials: Stress, Defect Formation and Surface Evolution*; Cambridge University Press: Cambridge, 2003.
- (3) Jacob, K. T.; Mathews, T. Phase Relations and Thermodynamic Properties of Condensed Phases in the System Sr-Cu-O. *J. Am. Ceram. Soc.* **1992**, *75*, 3225.
- (4) Hiroi, Z.; Takano, M. High-pressure synthesis as a promising method to search for new materials. *Physica C* **1994**, *235*.
- (5) Moiseeva, G.; Šestá, J.; Jzakovski, V.; Garipova, I.; Ilynych, N. Some calculation methods as a tool to revise thermodynamic data for the SrCuO_2 , Sr_2CuO_3 , $\text{Sr}_{14}\text{Cu}_{24}\text{O}_{41}$ and SrCu_2O_2 double oxides. *Thermochimica Acta* **1998**, *318*, 201.

- (41) Krockenberger, Y.; Ikeda, A.; Kumakura, K.; Yamamoto, H. Infinite-layer phase formation in the $\text{Ca}_{1-x}\text{Sr}_x\text{CuO}_2$ system by reactive molecular beam epitaxy. *J. Appl. Phys.* **2018**, *124*, 073905.
- (42) Pauling, L. The principles determining the structure of complex ionic crystals. *J. Amer. Chem. Soc.* **1929**, *51*, 1010., Pauling, L. *The nature of the chemical bond and the structure of molecules and crystals: an introduction to modern structural chemistry*, 3rd ed.; Cornell University Press: New York, 1960.
- (7) Little, S.; Zangwill, A. Equilibrium microstructure of epitaxial thin films. *Phys. Rev. B* **1994**, *49*, 16659.
- (9) Matthews, J. W. Defects associated with the accommodation of misfit between crystals. *J. Vac. Sci. Tech.* **1975**, *12*, 126.
- (45) Rosner, H.; Hayn, R.; Schulenburg, J. Tight-binding parameters and exchange integrals of $\text{Ba}_2\text{Cu}_3\text{O}_4\text{Cl}_2$. *Phys. Rev. B* **1998**, *57*, 13660.
- (46) Ueno, K.; Shimotani, H.; Yuan, H.; Ye, J.; Kawasaki, M.; Iwasa, Y. Field-Induced Superconductivity in Electric Double Layer Transistors. *J. Phys. Soc. Jpn.* **2014**, *83*, 032001.

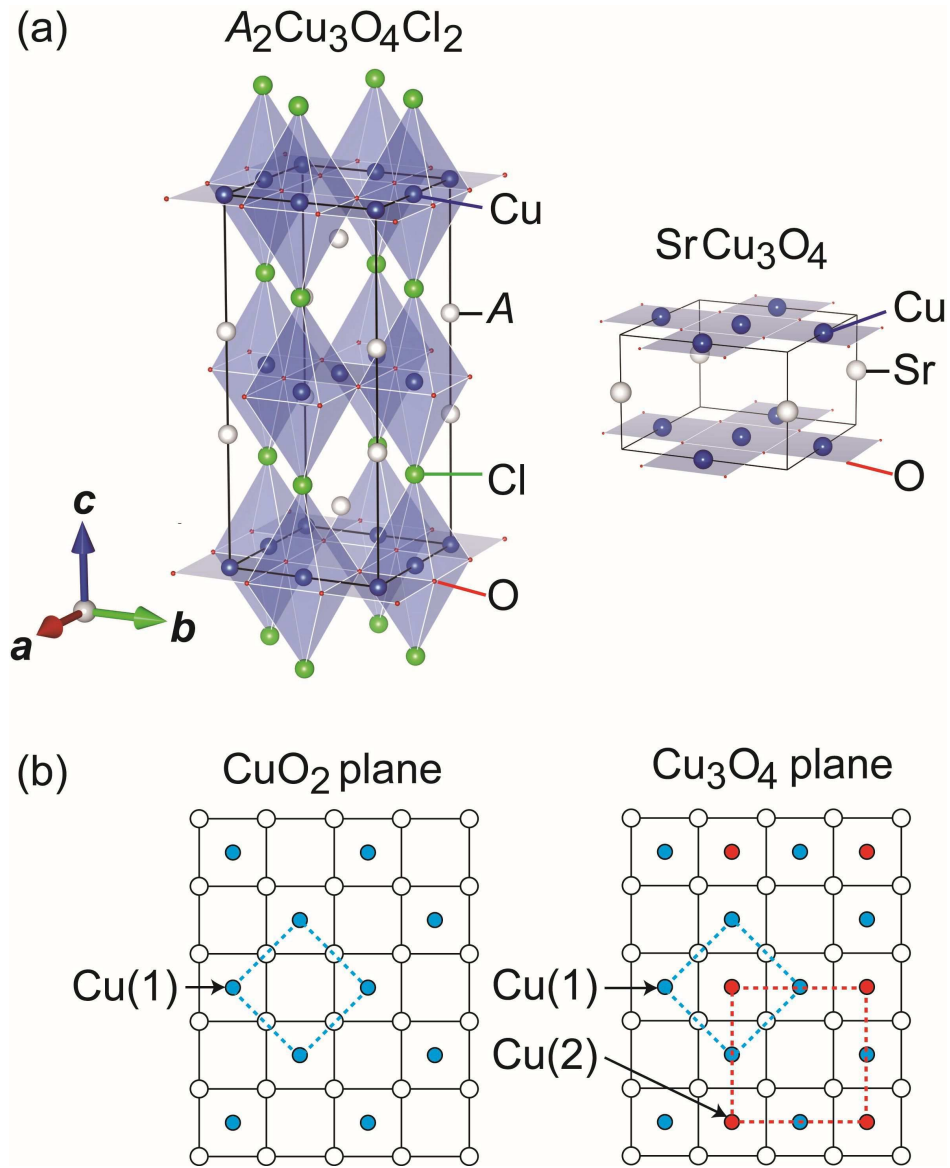


Figure 1: (a) Crystal structures of $A_2Cu_3O_4Cl_2$ ($A = Sr, Ba$) (left) and $SrCu_3O_4$ (right) with Cu_3O_4 ($Cu_{3/2}O_2$) planes. (b) The pristine CuO_2 plane with apex-linked CuO_4 units (left) and the Cu_3O_4 plane with edge-linked CuO_4 units (right) showing interpenetrating square lattices by $Cu(1)$ and $Cu(2)$ (dashed lines).

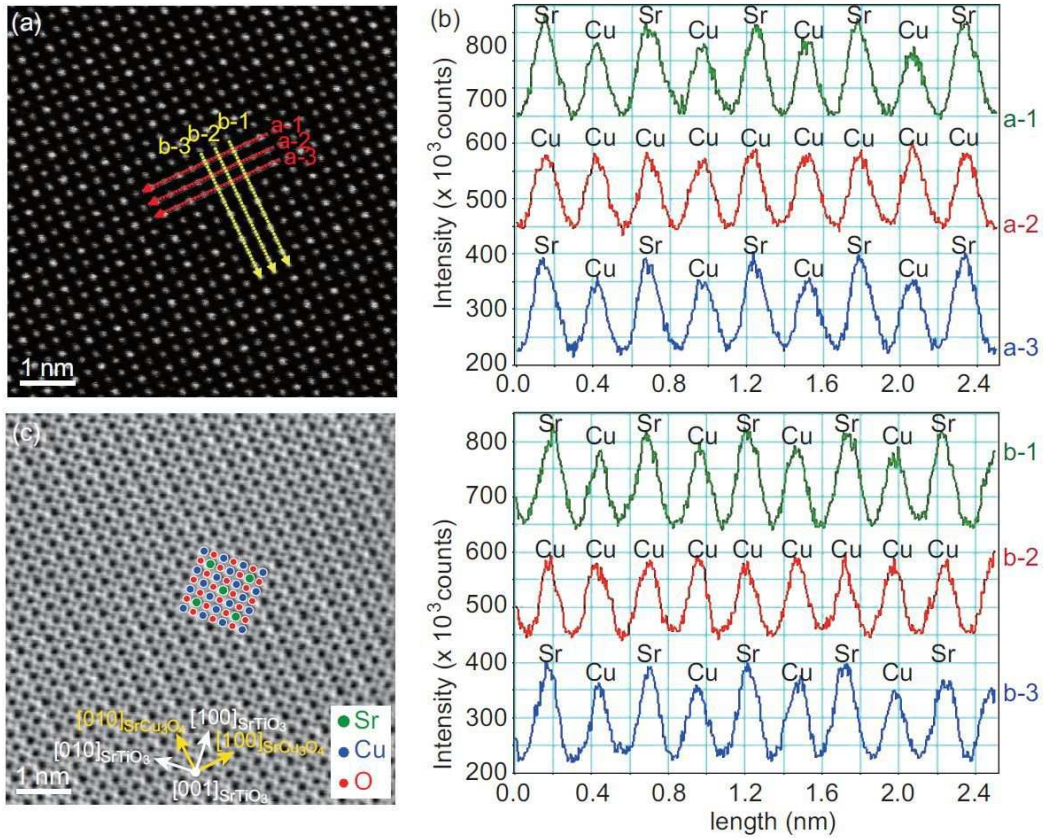


Figure 2: (a) High resolution HAADF-STEM image of the film with 30 nm thickness taken at RT. (b) Line scans along lines a-*i* (*i* = 1, 2, 3) (top) and those along lines b-*i* (*i* = 1, 2, 3) (bottom) shown in (a). (c) ABF-STEM image.

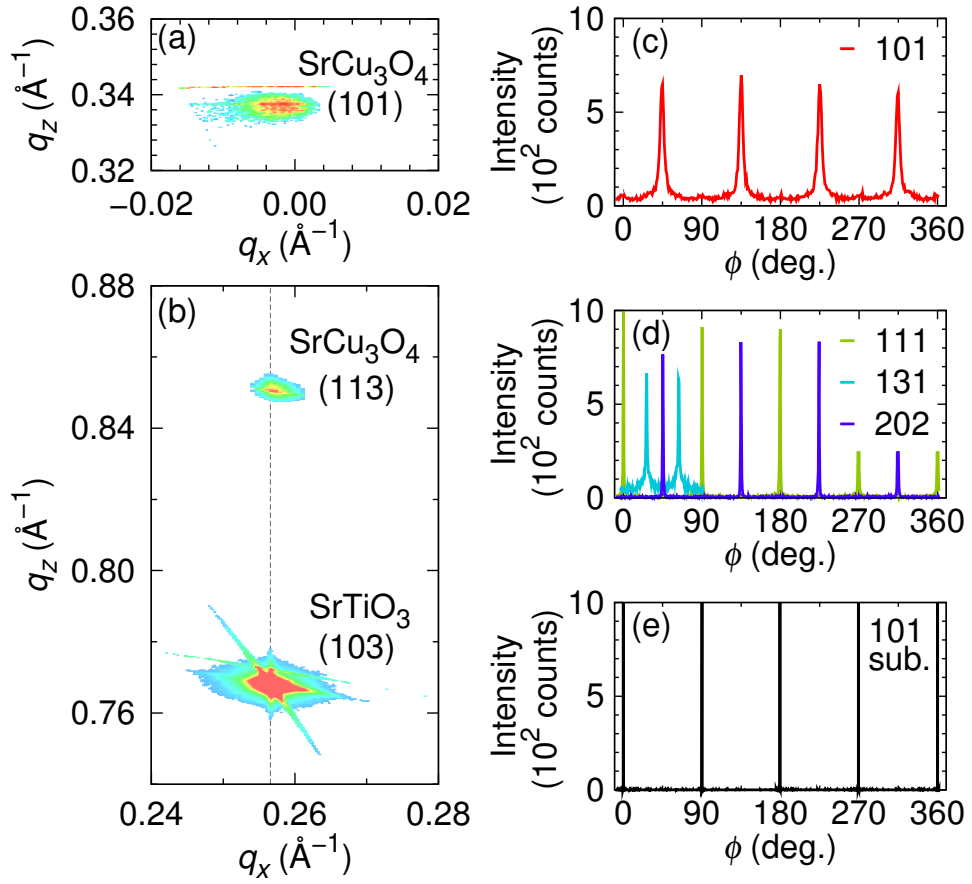


Figure 3: (a)–(b) X-ray reciprocal space mappings around 101 and 113 of the SrCu_3O_4 film. (c)–(e) ϕ scans of the 101 reflection of the SrTiO_3 substrate and representative peaks of the film.

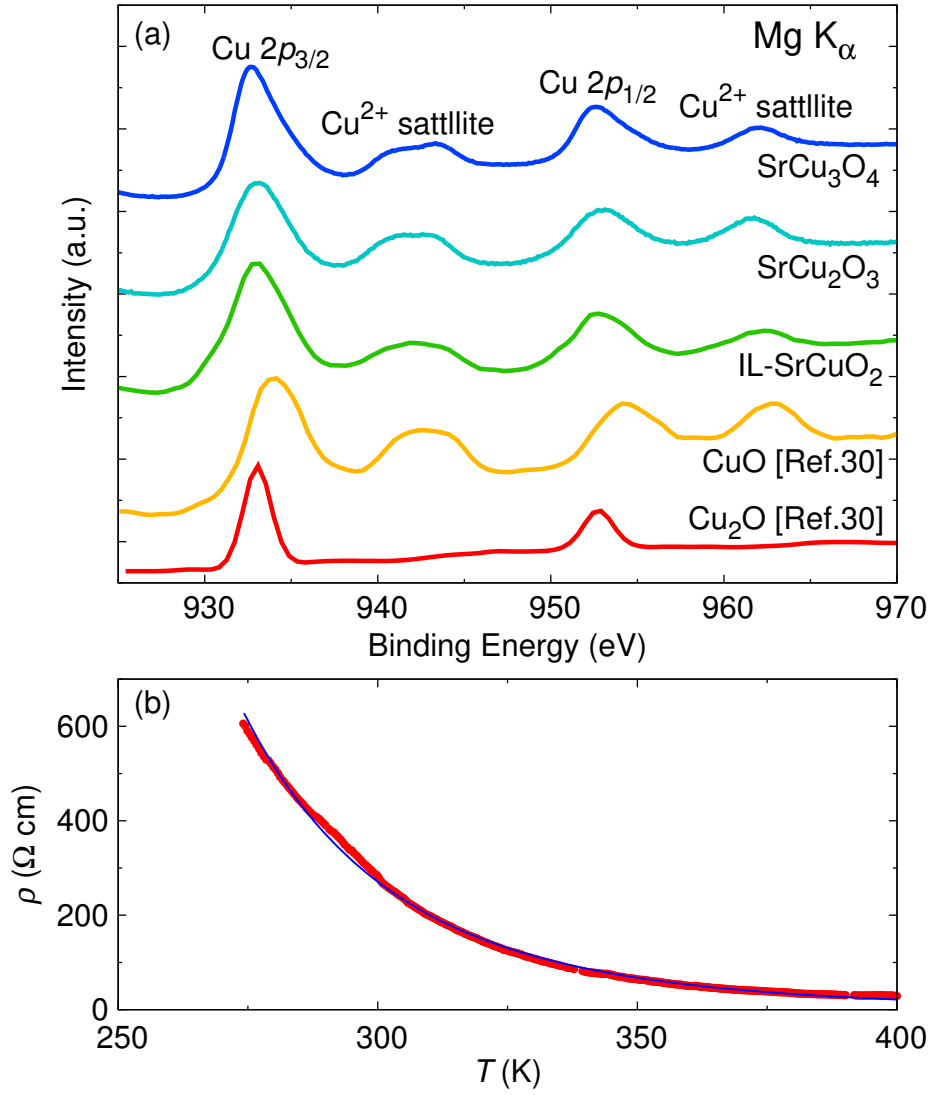


Figure 4: (a) XPS Cu 2p core-level spectra of the SrCu₃O₄ film and several copper oxides. (b) Temperature dependence of electrical resistivity ρ of the SrCu₃O₄ film. The solid line represents the variable range hopping model for 2D (see text).

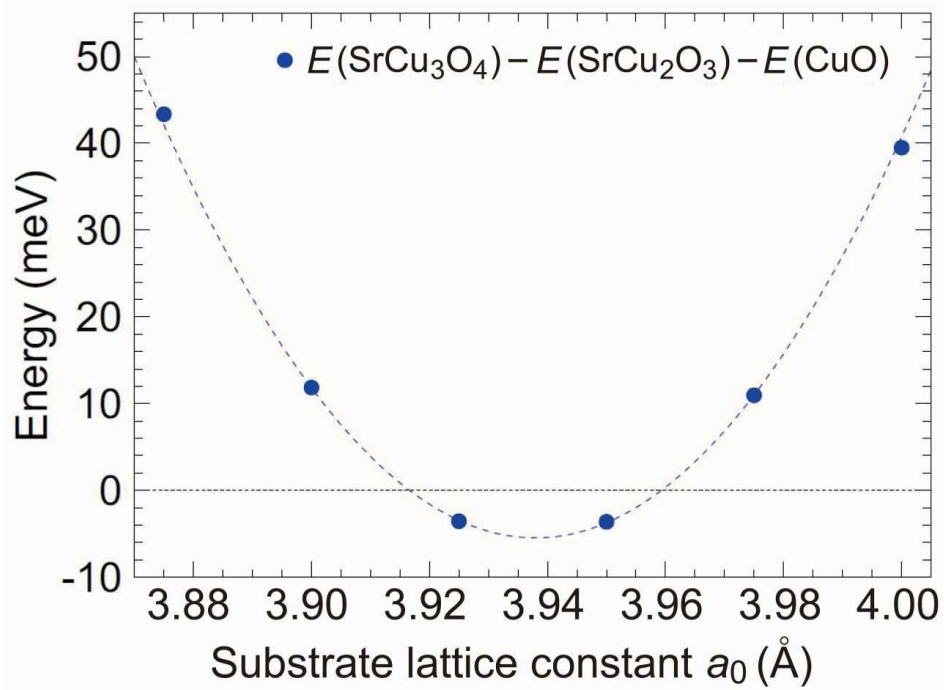


Figure 5: Energy difference between the calculated total energy of SrCu_3O_4 and that of $\text{SrCu}_2\text{O}_3 + \text{CuO}$ under the epitaxial strain, where a_0 is the in-plane lattice constant of the substrate. We assumed the fixed in-plane lattice constants $a = b = \sqrt{2}a_0$ for SrCu_3O_4 and $a = c = a_0$ for SrCu_2O_3 . This line is the guide to the eye.

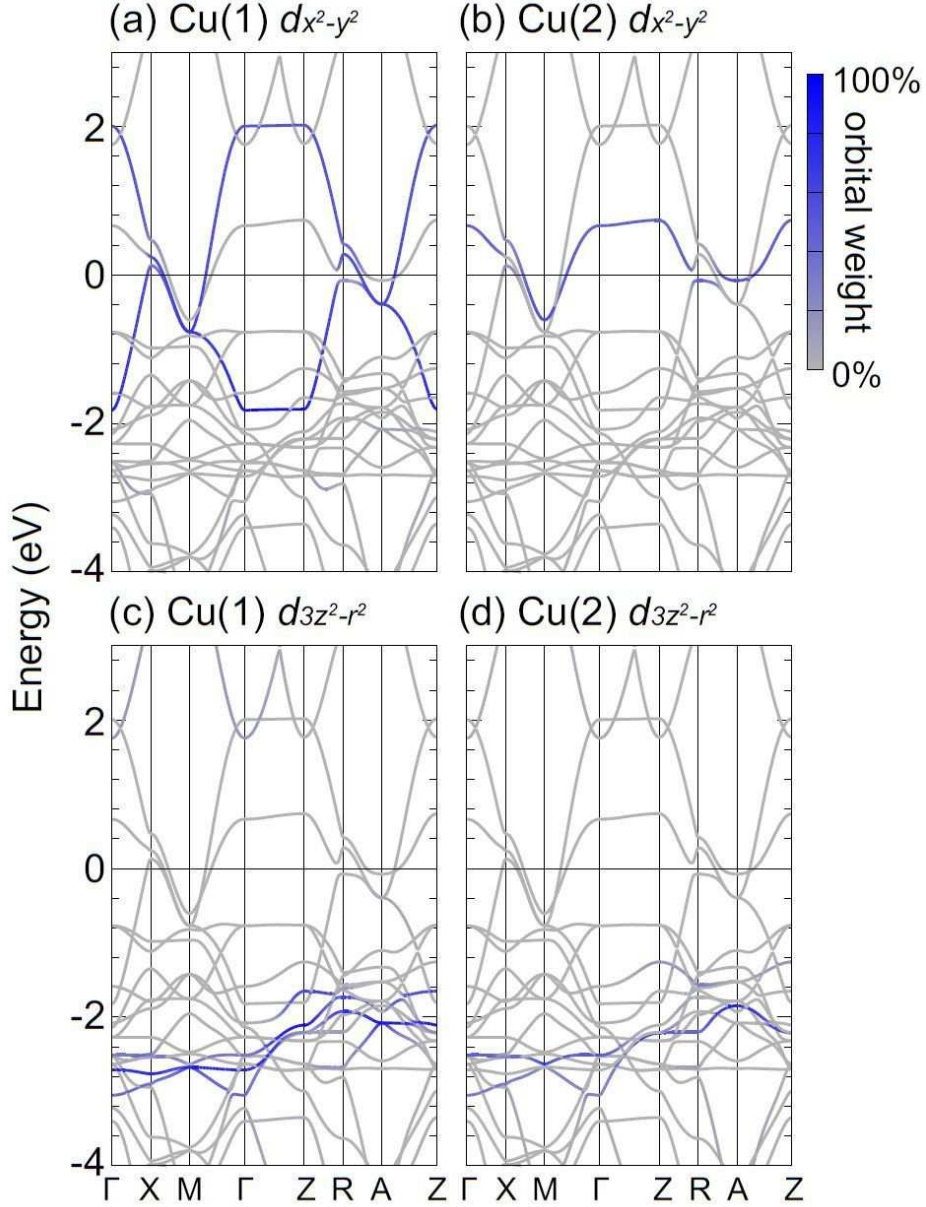
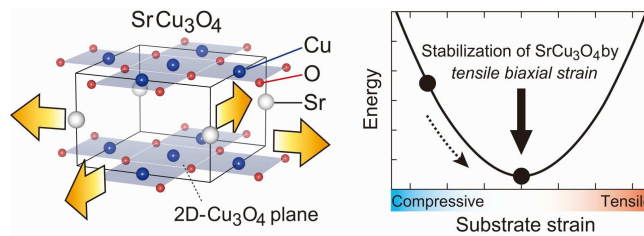


Figure 6: Calculated electronic band structure of SrCu_3O_4 with (a) Cu(1) $d_{x^2-y^2}$, (b) Cu(2) $d_{x^2-y^2}$, (c) Cu(1) $d_{3z^2-r^2}$, and (d) Cu(2) $d_{3z^2-r^2}$ orbitals highlighted in blue. The Fermi energy is set at zero. Note that the notation of $d_{x^2-y^2}$ is used here in accordance with the usual manner of cuprates, while d_{xy} is a more suitable notation to the present case since the ab axes of SrCu_3O_4 are rotated by 45° from the xy axes used in the calculations; i.e., the in-plane structure of SrCu_3O_4 is expanded to $\sqrt{2}a \times \sqrt{2}a$ with respect to IL-SrCuO_2 .

TOC graphic and synopsis

We prepared epitaxial SrCu_3O_4 thin films with infinitely stacked Cu_3O_4 layers composed of edge-sharing CuO_4 square-planes, using molecular beam epitaxy. Experimental and theoretical characterizations revealed that SrCu_3O_4 can exist under tensile biaxial strain from the (001)- SrTiO_3 substrate. This material is a suitable system for electron doped superconductivity based on the Cu_3O_4 plane.



For Table of Contents Only

Supporting Information of “Epitaxial stabilization of SrCu₃O₄ with infinite Cu_{3/2}O₂ layers”

Abstract

In this supporting information, we present X-ray diffraction (XRD), experimental and calculation results of electron diffraction (ED) for SrCu₃O₄ films grown on the (001)-SrTiO₃ substrate. We also show results of high-angle annular dark-field scanning transmission electron microscopy (HAADF-STEM) for thick (30 nm) films, and X-ray photoelectron spectroscopy (XPS) for the thin (5 nm) and thick (30 nm) films. In addition, we present the first principles calculation of the phonon dispersion of SrCu₃O₄ with the experimental lattice constants ($a = 5.42 \text{ \AA}$ and $c = 3.53 \text{ \AA}$).

XRD analysis of the SrCu₃O₄ film on the SrTiO₃ substrate

Figure S1 shows the out-of-plane θ - 2θ XRD pattern for the film on the (001)-oriented SrTiO₃ substrate grown in the present optimal growth condition ($T = 472^\circ\text{C}$, nominal ratio of Cu/Sr = 2, and O₃ gas flow with a background pressure of 4×10^{-6} Torr). Sharp peaks with distinct fringes were observed around $2\theta = 25^\circ$ and 52° , suggesting the successful growth of a well-oriented and excellent quality film, although a tiny unknown peak is present at around 42° . A film thickness is estimated from the spacing of fringes to be about 30 nm, which agrees with the estimation from the growth rate. The inset shows the rocking curve of the peak around 25° , showing a full width at half-maximum of $\Delta\omega = 0.09^\circ$. In Table 1, we summarized structural parameters of SrCu₃O₄.

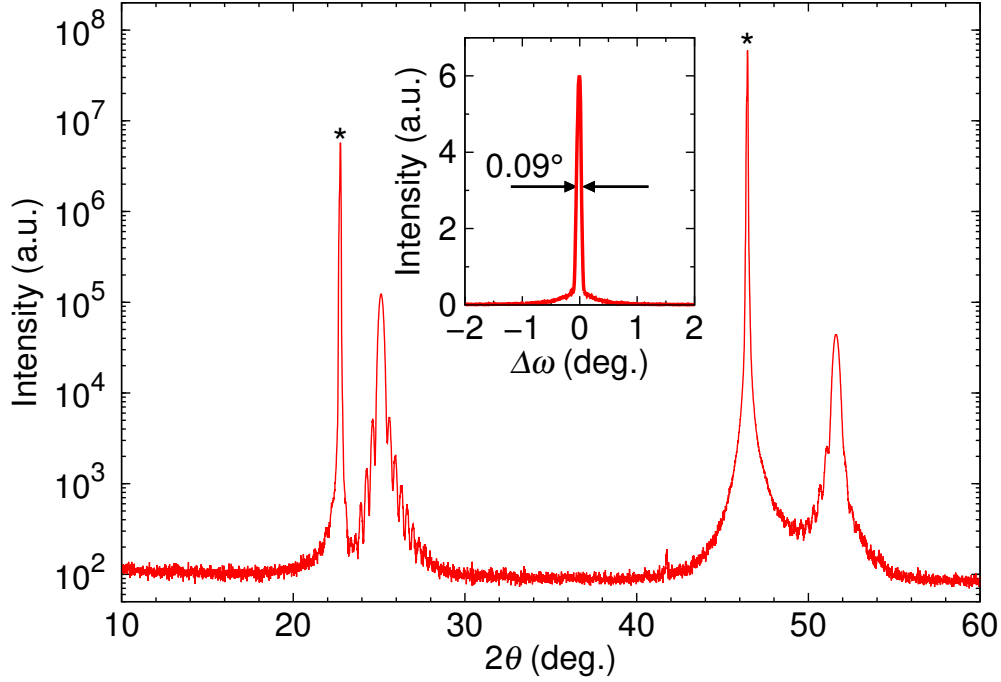


Figure S1: Out-of-plane θ - 2θ XRD patterns of films with a 30 nm thickness. SrTiO₃ substrate peaks are marked with asterisks. Inset shows rocking curve of the peak around 25°.

Growth of films on other substrates

We also performed experiments using other substrates than SrTiO₃, such as the (001)-oriented KTaO₃ and (110)-oriented DyScO₃ substrates under the present optimal growth condition for the growth of SrCu₃O₄ films on the SrTiO₃ substrate. For these KTaO₃ and DyScO₃ substrates, one can expect larger tensile strain than the SrTiO₃ substrate for SrCu₃O₄ (see the inset of Figure S2).^{S1} However, we did not obtain the single phase of SrCu₃O₄ on these substrates, respectively. Using the KTaO₃ substrate, we obtained a film containing three phases such as *c*-axis oriented SrCu₂O₃, *a*-axis oriented Sr₁₄Cu₂₄O₄₁, and possibly *c*-axis oriented SrCu₃O₄ (Figure S2). On the other hand, using the DyScO₃ substrate, we obtained a film containing two phases such as *c*-axis oriented SrCu₂O₃, and *a*-axis oriented Sr₁₄Cu₂₄O₄₁, although XRD intensities of these phases are very small (Figure S2). Since DyScO₃ has a pseudo-cubic structure,^{S2} it is also possible that SrCu₃O₄ could not be obtained due to anisotropic strain. The obtained phases here are determined by XRD peak

Table 1: Structural parameters for the thin film of SrCu_3O_4 . The space group: $P4/mmm$ (No. 123); lattice constants: $a = 5.42 \text{ \AA}$, and $c = 3.53 \text{ \AA}$.

Atom	Site	x	y	z
Sr	1b	0	0	1/2
Cu	1c	1/2	1/2	0
Cu	2f	0	1/2	0
O	4j	0.25	0.25	0

positions of Sr-Cu-O compounds.^{S3-S5} We discuss more details of the strain effect for the synthesis of SrCu_3O_4 in the main text of this paper.

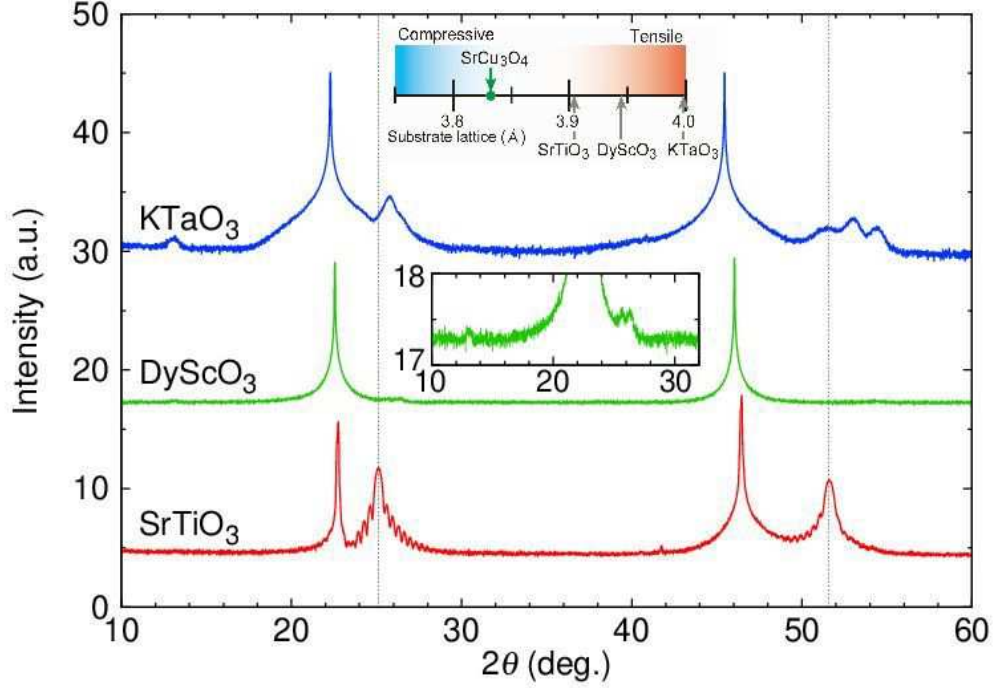


Figure S2: Out-of-plane θ - 2θ XRD patterns of films on the SrTiO₃, DyScO₃, and KTaO₃ substrates. The upper inset shows the relation between the substrate lattice constant and the in-plane lattice constant of SrCu₃O₄ divided by $\sqrt{2}$. The lower inset shows the enlarged XRD data of the film on the DyScO₃ substrate. Vertical dot lines indicate peak positions of SrCu₃O₄.

Experiments and calculations for ED of the SrCu₃O₄ film

In Figure S3a, we present experimental ED patterns for the same SrCu₃O₄ film as shown in Figure 2 of the main text. One can clearly see that the in-plane structure has a four-fold symmetry. The in-plane lattice constant is estimated as $a = 5.42 \text{ \AA}$. This observation is in good agreement with the calculation of the ED pattern (Figure S3b), assuming the tetragonal unit cell of the given structure of SrCu₃O₄ (see the right panel of Figure 1a of the main text and Table 1). We summarized observed and calculated d_{hkl} parameters in Table 2.

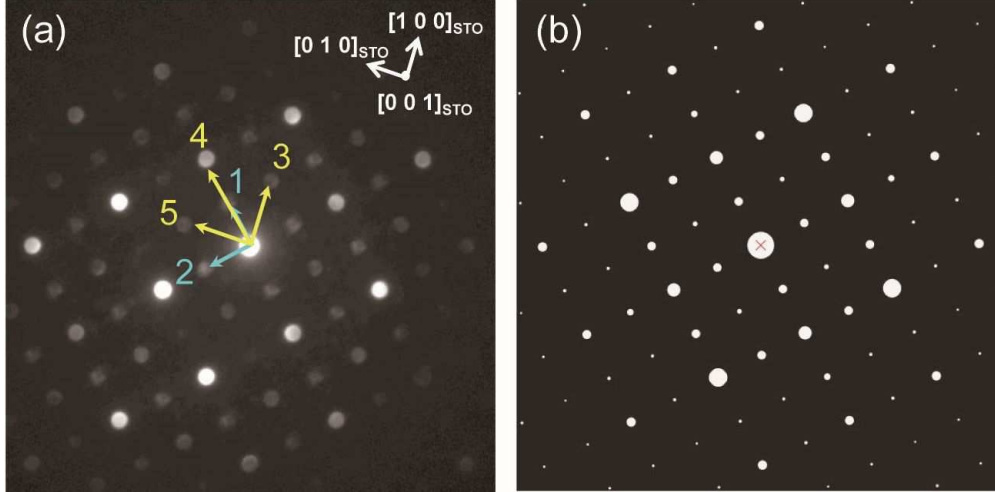


Figure S3: (a) Electron diffraction pattern of the film taken at room temperature along $[001]$. (b) Calculated pattern of electron diffraction, assuming a tetragonal structure with the in-plane lattice constant of $5.42\ \text{\AA}$.

Table 2: Observed and calculated d_{hkl} for representative ED spots. Numbers correspond to spot numbers in Figure S2a.

No.	measured d_{hkl} (nm)	calculated d_{hkl} (nm)	hkl
1	0.541	0.542	100
2	0.543	0.542	010
3	0.384	0.383	$1\bar{1}0$
4	0.271	0.271	200
5	0.384	0.383	110

Growth condition and reproducibility of the SrCu_3O_4 growth

For the determination of optimal growth conditions, we performed experiments by changing temperature and the flow rate of O_3 gas. In Table 3, we summarized the results of the synthesis of SrCu_3O_4 on the SrTiO_3 substrate at various temperatures and background pressures at a Cu/Sr ratio of 2. Here, the quality of the film was checked by XRD peak positions, fringes in the out-of-plane θ - 2θ XRD scan, impurities and multiple phases. In the present study, the optimal growth condition for the SrTiO_3 substrate was $472 \pm 1^\circ\text{C}$ and 4×10^{-6} Torr at a nominal Cu/Sr ratio of 2. Note that in the same temperature and pressure conditions, the single phase of SrCu_3O_4 was not obtained at different Cu/Sr ratios such as

Table 3: Summary of the growth conditions (temperature and background pressure) for SrCu₃O₄ films, with a nominal Cu/Sr ratio of 2. Double circles indicate that the XRD data showed the expected peaks and fringes. A single circle means that the film possesses the expected peaks, but no fringe is present. Triangles indicate the inclusion of multiple phases, including SrCu₃O₄, and crosses indicate the absence of peaks from SrCu₃O₄.

$T(\text{K})/P(\text{Torr})$	3.0×10^{-6}	3.5×10^{-6}	4.0×10^{-6}	5.0×10^{-6}
440	-	×	-	-
450	-	×	-	-
455-458	-	×	×	-
460	-	×	×	-
461-463	×	×	×	-
465	-	-	△	-
470-471	-	△	△	-
472-473	-	⊙	⊙	○
473-474	-	○	○	-
475	-	-	△	-
475-477	-	-	△	-
480-482	-	-	×	-

Cu/Sr = 1, 1.5, 1.7 and 2.3.

We observed the generation of non-crystalline phases and/or Sr₁₄Cu₂₄O₄₁ with some impurity phases when growth conditions are deviated from the optimal condition. For example, in the case of Cu/Sr = 1, SrCuO₂ with the infinite CuO₂ layer structure was obtained. The excess Sr condition for the growth of SrCu₃O₄ implies that the initially formed SrCu₂O₃ may be reconstructed to SrCu₃O₄ owing to the substrate strain as discussed in the main text, or re-evaporation of Sr from the film surface may take place.

The synthesis of SrCu₃O₄ is highly reproducible; using the present optimal growth condition and the (001)-SrTiO₃ substrate, we have succeeded in synthesizing SrCu₃O₄ in more than 10 times. It is noted that, to maintain the stability of temperature and monitoring condition, we synthesized the films at a fixed position without rotating the substrates. Al-

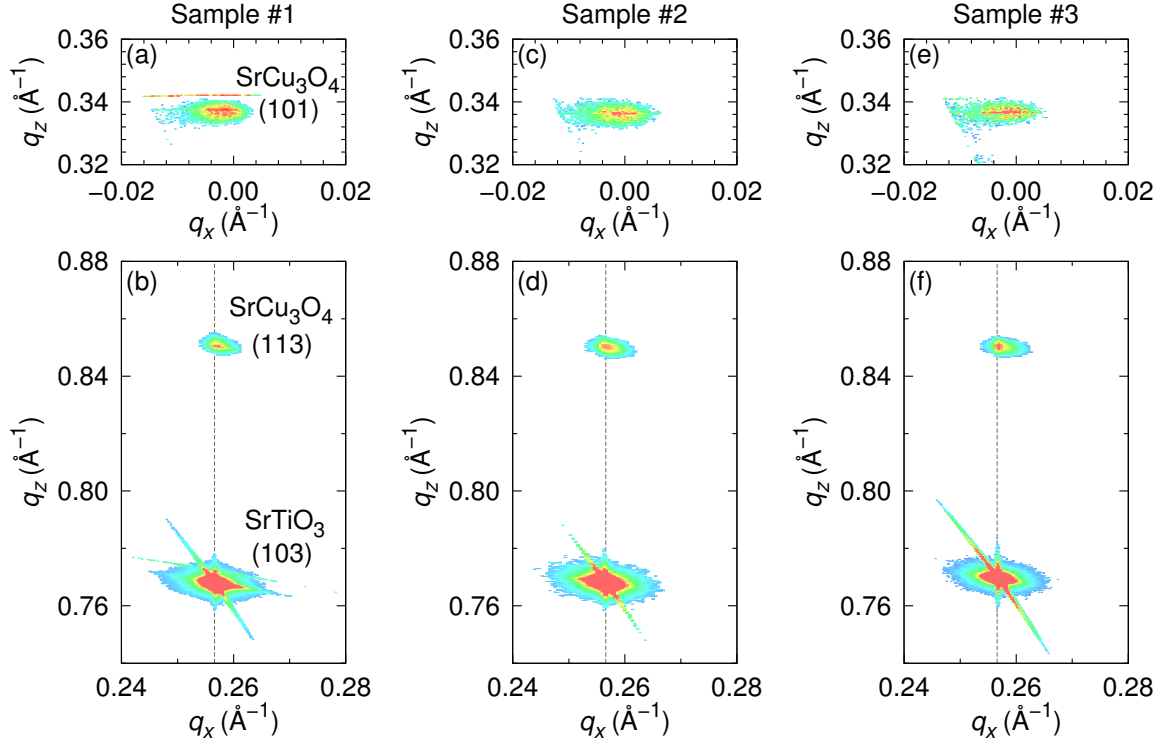


Figure S4: X-ray reciprocal space mappings around (a), (c), (e) 101 and (b), (d), (f) 113 for three different films of SrCu_3O_4 . The thicknesses of these films is almost the same (~ 30 nm). The coherent and reproducible growth of these films is confirmed.

most the same coherent feature of obtained films was confirmed in reciprocal space mapping of XRD measurements (Figure S4).

Multiple domain formation in thick films of SrCu_3O_4

A small portion of competing phases of SrCu_2O_3 and CuO was found in HAADF-STEM data for thicker films (> 30 nm), as shown in Figures S5a and S5b. Competing impurity phases were also detected as spot-like features in the RHEED pattern. A typical RHEED image for the film with a 5 nm thickness shows streaky patterns (Figure S5c), suggesting an extremely flat surface of the SrCu_3O_4 film. However, further growth under the same condition resulted in spot-like features along with the original streaks (Figure S5d), suggesting the formation of islands of extra phases that coexist with the epitaxially grown phase.

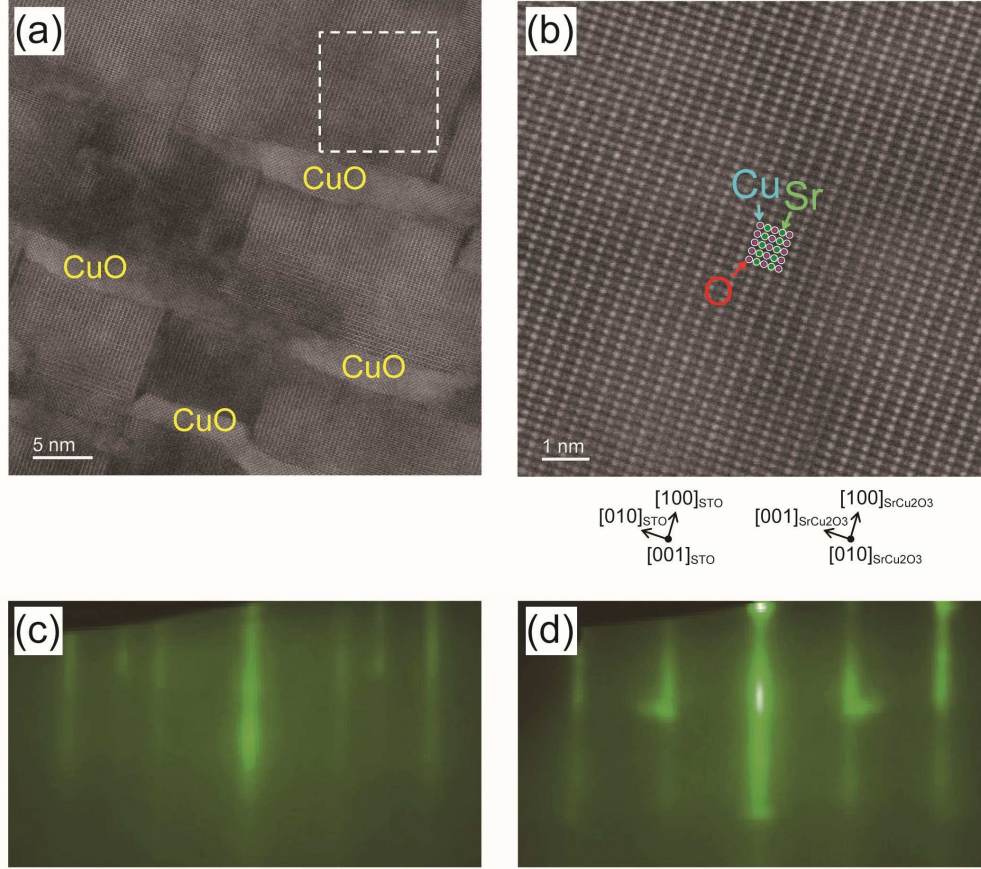


Figure S5: (a) HAADF-STEM image of an island of secondary phases in a thick film with 30 nm. Secondary phases were identified as b-axis oriented SrCu_2O_3 and CuO . (b) Magnified view for the white square region in (a). (c) RHEED images along the $[100]$ direction of the SrTiO_3 substrate for the samples with 5 nm thickness and (d) 30 nm thickness.

Figure S6 shows the $2p$ core level of Cu for SrCu_3O_4 films on the (001) - SrTiO_3 substrate. The film with 5 nm thickness is the same sample as shown in Figure 4a of the main text. Here we also show the result of a thicker film with 30 nm. For the thin film with 5 nm, we observed distinct satellite peaks, separated by ~ 9 eV, which are ascribed to the divalent copper state.^{S6} However, intensities of the satellites decreased in the thicker film with 30 nm. This result is probably due to impurity phases in the surface state, which appear in thicker films than 30 nm.

A phase mixture of SrCu_3O_4 and other phases can be understood as a consequence of multiple domain formation that reduces the stress from the substrate.^{S7,S8} This result implies

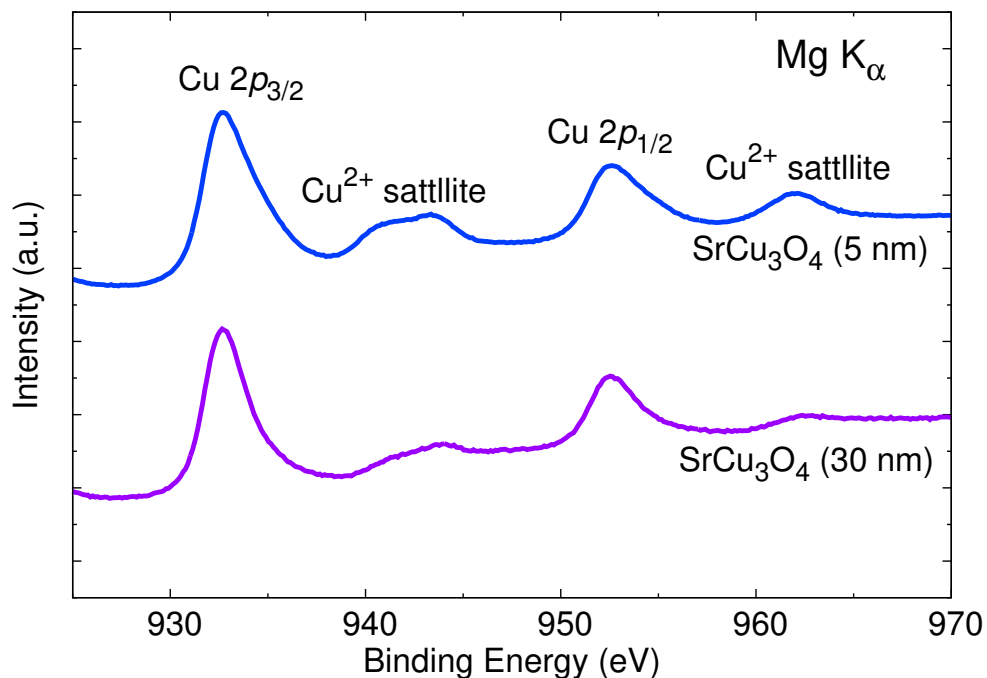


Figure S6: Cu $2p$ core level XPS spectra of SrCu_3O_4 films with 5 nm and 30 nm thickness.

that the epitaxially stable phase (SrCu_3O_4) and secondary phases (SrCu_2O_3 and CuO) are both thermodynamically stable,^{S7} however, the former phase cannot appear in bulk owing to competing secondary phases that are more stable in bulk. The multiple domain formation is another strain relaxation mechanism different from misfit dislocation.^{S9,S10}

Calculated phonon dispersion of SrCu₃O₄

The phonon dispersion of SrCu₃O₄ calculated using the experimentally observed lattice constants of $a = 5.42 \text{ \AA}$ and $c = 3.53 \text{ \AA}$ is shown in Figure S7. No imaginary modes are present, suggesting that SrCu₃O₄ is dynamically stable. This result is consistent with the experimental observation of the multiple domain formation for thick films of SrCu₃O₄ (Figures S5 and S6); that is, SrCu₃O₄ is considered thermodynamically stable.

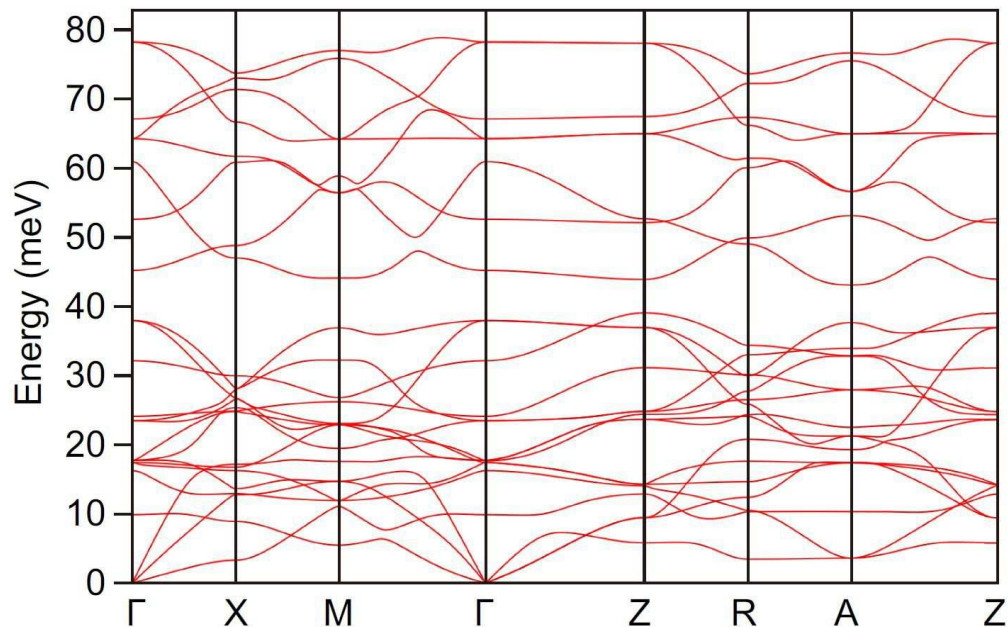


Figure S7: Phonon dispersion of SrCu₃O₄ obtained by first-principles calculation using the lattice constants of the thin film ($a = 5.42 \text{ \AA}$ and $c = 3.53 \text{ \AA}$).

References

- [S1] Schlom, D. G.; Chen, L.-Q.; Fennie, C. J.; Gopalan, V.; Muller, D. A.; Pan, X.; Ramesh, R.; Uecker, R. Elastic strain engineering of ferroic oxides. *MRS Bulletin* **2014**, *39*, 118.
- [S2] Velickov, B.; Kahlenberg, V.; Bertram, R.; Bernhagen, M. Crystal chemistry of GdScO₃, DyScO₃, SmScO₃ and NdScO₃. *Z. Kristallogr.* **2007**, *222*, 466.

- [S3] Jacob, K. T.; Mathews, T. Phase Relations and Thermodynamic Properties of Condensed Phases in the System Sr-Cu-O. *J. Am. Ceram. Soc.* **1992**, *75*, 3225.
- [S4] Hiroi, Z.; Takano, M. High-pressure synthesis as a promising method to search for new materials. *Physica C* **1994**, *235*.
- [S5] Moiseeva, G.; Šestá, J.; Jzukovski, V.; Garipova, I.; Ilynych, N. Some calculation methods as a tool to revise thermodynamic data for the SrCuO₂, Sr₂CuO₃, Sr₁₄Cu₂₄O₄₁ and SrCu₂O₂ double oxides. *Thermochimica Acta* **1998**, *318*, 201.
- [S6] Hayez, V.; Franquet, A.; Hubin, A.; Terryn, H. XPS study of the atmospheric corrosion of copper alloys of archaeological interest. *Surf. Interface Anal.* **2004**, *36*, 876.
- [S7] Little, S.; Zangwill, A. Equilibrium microstructure of epitaxial thin films. *Phys. Rev. B* **1994**, *49*, 16659.
- [S8] Gorbenko, O. Y.; Samoilenkov, S. V.; Graboy, I. E.; Kaul, A. R. Epitaxial Stabilization of Oxides in Thin Films. *Chem. Mater* **2002**, *14*, 4026.
- [S9] Matthews, J. W. Defects associated with the accommodation of misfit between crystals. *J. Vac. Sci. Tech.* **1975**, *12*, 126.
- [S10] Freund, L. B.; Suresh, S. *Thin Film Materials: Stress, Defect Formation and Surface Evolution*; Cambridge University Press: Cambridge, 2003.